The Development of a Biologically Inspired Propulsor for Unmanned Underwater Vehicles

James Louis Tangorra, *Member, IEEE*, S. Naomi Davidson, Ian W. Hunter, Peter G. A. Madden, George V. Lauder, Haibo Dong, Meliha Bozkurttas, and Rajat Mittal

***Abstract*—Fish are remarkable in their ability to maneuver and to control their body position. This ability is the result of the coordinated movement of fins which extend from the body and form control surfaces that can create and vector forces in 3-D. We have embarked on a research program designed to develop a maneuvering propulsor for unmanned undersea vehicles (UUVs) that is based on the pectoral fin of the bluegill sunfish. For this, the anatomy, kinematics, and hydrodynamics of the sunfish pectoral fin were investigated experimentally and through the use of computational fluid dynamics (CFD) simulations. These studies identified that the kinematics of the sunfish pectoral fin are very complex and are not easily described by traditional "rowing"- and "flapping"-type kinematics. A consequence of the complex motion is that the pectoral fin can produce forward thrust during both its outstroke (abduction) and instroke (adduction), and while doing so generates only small lateral and lift forces. The results of the biological studies were used to guide the design of robotic pectoral fins which were built as experimental devices and used to investigate the mechanisms of thrust production and control. Because of a design that was based heavily on the anatomy of the sunfish fin, the robotic pectoral fins had the level of control and degrees of freedom necessary to reproduce many of the complex fin motions used by the sunfish during steady swimming. These robotic fins are excellent experimental tools, and are an important first step towards developing propulsive devices that will give the next generation of UUVs the ability to produce and control thrust like highly maneuverable fish.**

***Index Terms*—Autonomous underwater vehicle (AUV), biorobotic, design, drag, pectoral fin, robotic, thrust, unmanned underwater vehicle (UUV).**

Manuscript received June 5, 2006; revised April 11, 2007; accepted April 22, 2007. This work was supported by the U.S. Office of Naval Research, Multiple University Research Initiative under Grant N000140310897.

Associate Editor: F. S. Hover.

J. L. Tangorra was with the Bioinstrumentation Laboratory, Massachusetts Institute of Technology, Cambridge, MA 02139 USA. He is now with the Drexel University, Philadelphia, PA 19104 USA (e-mail: jtangor@mit.edu).

S. N. Davidson was with the Bioinstrumentation Laboratory, Massachusetts Institute of Technology, Cambridge, MA 02139 USA. She is now with the McKinsey and Company, San Francisco, CA 94104 USA.

I. W. Hunter is with the Bioinstrumentation Laboratory, Massachusetts Institute of Technology, Cambridge, MA 02139 USA.

P. G. A. Madden was with the Harvard University, Cambridge, MA 02139 USA. He is now with the Evergreen Solar, Inc., Marlboro, MA 01752-3016 USA.

G. V. Lauder is with the Harvard University, Cambridge, MA 02139 USA.

H. Dong was with The George Washington University, Washington, DC 20052 USA. He is now with the Department of Mechanical and Materials Engineering, Wright State University, Dayton, OH 45435 USA.

M. Bozkurttas was with The George Washington University, Washington, DC 20052 USA. She is now with the Exa Corporation, Burlington, MA 01803 USA.

R. Mittal is with the Department of Mechanical and Aerospace Engineering, The George Washington University, Washington, DC 20052 USA.

Digital Object Identifier 10.1109/JOE.2007.903362

Fig. 1. Bluegill sunfish with right pectoral fin extended.

I. Introduction

The use of unmanned undersea vehicles (UUVs) for underwater surveillance, salvage, research, and military missions is becoming increasingly common. The maneuverability and control of UUVs during such operations is an obvious concern. Typically, UUVs have rigid bodies, are driven using propellers, and produce their maneuvering forces with rigid control surfaces that are effective only when the flow of the water past the UUV exceeds a minimum velocity. In contrast, fish, which are remarkable in their ability to maneuver and to control their body position, have, with few exceptions, flexible bodies, and use flexible fins that are actively controlled to make the appropriate movement and assume the appropriate shape for generating the forces required by a particular situation (e.g., maneuvers, hovering, high-speed stability, and braking) [1], [2]. Recently, some UUVs have been built which use oscillating foils that approximate the rowing and flapping movements exhibited by the fins of some marine animals [3]–[5]. Nonetheless, the complexity of motion, degrees of freedom, and level of control that are associated with fish swimming have yet to be matched and exploited by an engineered system for the maneuvering and propulsion of UUVs.

We have undertaken a research program designed to develop a maneuvering propulsor for UUVs that is based on the pectoral fin of the bluegill sunfish (*Lepomis macrochirus*, Fig. 1). Bluegill sunfish are highly maneuverable bony fishes that have been the subject of numerous experimental analyses of locomotor function [6]–[9]. Although swimming generally involves the coordinated movement of many fin surfaces, the sunfish is capable of propulsion and maneuvering using almost exclusively the pectoral fins. They are able to hover, brake, spin along their long axis, execute yaw maneuvers, and propel themselves

forward and backwards at low speeds [10], [11]. These abilities are the direct result of the pectoral fins being highly conformable control surfaces that can create and vector thrust in 3-D. It is believed that by understanding these complex, highly controlled movements, and by borrowing appropriately from the pectoral fin's design, a human engineered propulsor can be developed to provide UUVs multidirectional thrust generation and superior levels of control.

This research program is using a four-part approach in the analysis and design of a propulsor based on principles derived from bluegill pectoral fin function. First, a detailed, biological study of the pectoral fin's anatomy, its mechanical properties, and the 3-D kinematics exhibited during locomotion were conducted. Second, the hydrodynamics of fins on freely swimming fishes was studied experimentally and through computational fluid dynamics (CFD) simulations to estimate the hydrodynamic forces and to characterize the flow and vortex patterns created by the fin. Third, robotic prototypes of the fin are being developed that can reproduce many of the complex motions used by the fin for propulsion and maneuvering. These prototypes are being used to understand better how the fin produces and controls its hydrodynamic forces, and to experiment with manufacturing, control, and actuation methods. Fourth, a suite of conducting polymer materials is being developed that will be incorporated as actuators, structural components, and power delivery mechanisms. It is recognized that to achieve a level of performance equal, or superior, to that of the fish fin, the final design will require actuators and actively controlled materials with properties and performance characteristics that exceed those of traditional devices [12].

This paper concentrates on the design and performance of our first generation biorobotic pectoral fins. The methods and results of the biologic and hydrodynamic studies that were used to inform the design are presented only briefly. The primary goal for this first prototype was to develop a device that produced a range of motions similar to that of the bluegill pectoral fin so that the mechanisms that contribute to the production and control of thrust could be better understood. A biorobotic fin was developed that borrowed from, but did not mimic, the architecture of the bluegill pectoral fin (Figs. 1 and 2). Flexible, bilaminar fin rays were embedded in a compliant webbing material that resembled the shape of the bluegill pectoral fin. The fin rays were seated onto a compliant base that acted as both a structural support and a hinge about which the fin rays could be moved. The fin rays were actuated via nylon tendons driven by servomotors. By using a compliant-mechanism-based design and fin rays that gave active control over the fin's shape, the biorobotic fin had the degrees of freedom and surface conformability required to reproduce sufficiently the complex fin motions that the bluegill sunfish uses during propulsion and maneuvering.

This paper is intended to serve as an introductory paper to a series of focused studies that will more rigorously address aspects of the biorobotic pectoral fin and its performance. A second generation fin design that is slightly less complex and that has more constraints on its motion has been developed and is being tested using experimental and numerical flow visualizations [e.g., particle image velocimetry (PIV) and CFD]. Hydrodynamic studies are being conducted to investigate how

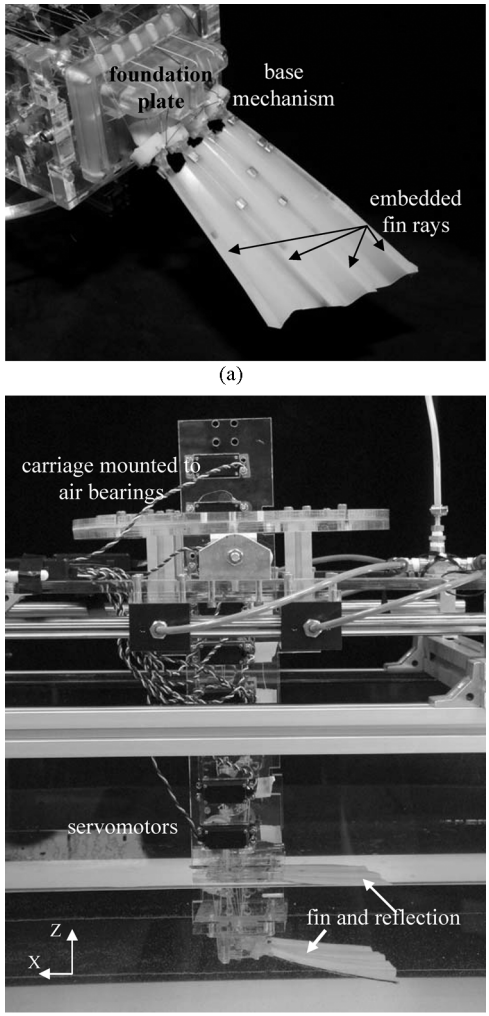

Fig. 2. (a) Biorobotic pectoral fin and (b) the fin mounted to an air-bearing carriage and placed in a testing tank. The fin web is 125 mm along the dorsal (right) edge, 85 mm along the ventral edge, and when relaxed, 55 mm across the base and 70 mm between the lateral tips of the ventral and dorsal edges. Web thickness ranges from approximately 1.0 mm between fin rays to 1.8 mm at, and including, the fin rays.

specific movements of the fin and the fin's spatially varying flexibility affect the resultant hydrodynamics and energy requirements. These results will be presented in future articles together with companion CFD analyses that allow us to more confidently attribute hydrodynamic events to particular characteristics of the fin and its motions.

II. Kinematics, Mechanical Properties, and Hydrodynamics

The fins of swimming marine animals have been the subject of many studies and have been used as inspiration for the development of fin-like propulsive and maneuvering foils for aquatic vehicles [3]–[5]. The kinematics of how fins are employed in nature [11], [13] and the forces and fluid dynamics of biomimetic foils have been studied extensively [14]–[19]. In these studies, fins are modeled generally as foils or paddles, with unsteady, oscillatory motions that are composed of a pitch about the fin's spanwise axis, a heave in the vertical, and a fore and aft rowing

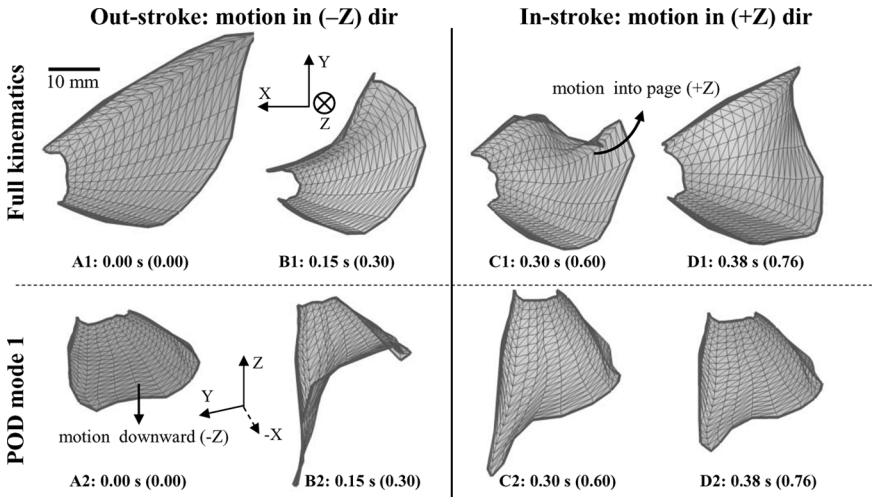

Fig. 3. Conformations of the sunfish pectoral fin at four times during the fin beat during steady swimming (top four images). The time stamp indicates the time within the fin's 0.50-s fin beat, and the number in parenthesis represent the decimal fraction of the fin cycle, with 1.00 representing the full cycle. The grayscale code reflects the distance from the body with darker gray indicating positions further from the fish body. Conformations of the fin for POD mode 1 are shown in the bottom four figures. The fin is shown from a perspective similar to that for images of the robotic fin during experimental testing.

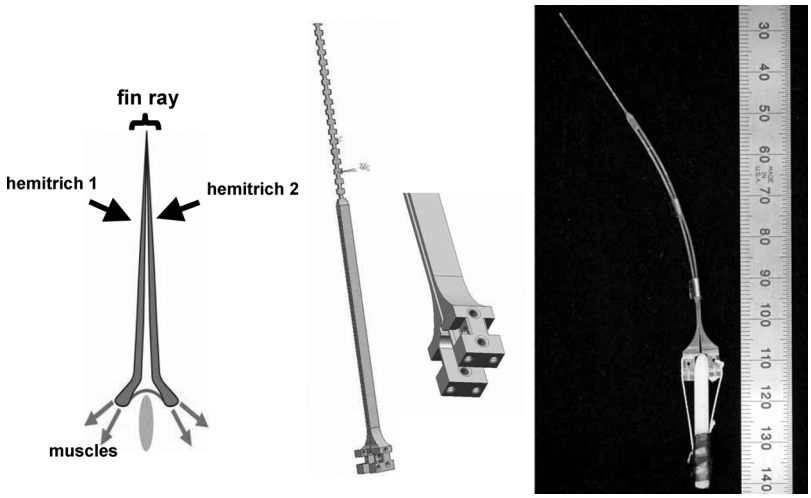

Fig. 4. Fin rays. (left) Schematic of the fish fin ray and (center and right) the fin rays for the biorobotic fin. Each fin ray in the sunfish possesses two segmented halves (hemitrichs) that are controlled by two pairs of muscles. The anatomy is approximated in the biorobotic fin rays which were manufactured using stereo lithography. A displacement of one hemitrich's base relative to the other by approximately 1.0 mm results in the deflection of the fin ray tip by approximately 35.0 mm.

motion. The motion of the bluegill sunfish pectoral fin, however, is very different from the simplified models that have been used as the basis for propulsors. The motions are highly complex and the kinematics and resultant fluid mechanics do not lend themselves easily to an analysis based on the pitching and heaving of a foil or the rowing of a paddle.

A. Kinematics

The motion of the sunfish pectoral fin during free swimming was studied by filming the fish with two spatially calibrated, high-speed video cameras, and by creating 3-D digital reconstructions of the fin's movements [20]. The high-speed video and digital reconstructions made clear that pectoral fin motion in 3-D is very complex and involves the following: 1) the simultaneous movement of the upper and lower edges of the fin away from the body, forming two simultaneous leading edges [Fig. 3(A1) and (A2)], 2) a strong cupping of the fin as it moves away from the body (abduction) [Fig. 3(B1) and (B2)], 3) a wave of bending that moves spanwise along the upper edge of the fin at a velocity higher than the free-stream flow velocity, 4) a dimpling of the fin's upper surface behind the leading edge [Fig. 3(C1) and (C2)], 5) a reorientation of the fin base and rotation of the fin, and 6) significant area changes during the cycle of the fin beat.

B. Mechanical Properties

The sunfish pectoral fin is composed of 14 bony fin rays sandwiched between two layers of a thin, compliant membrane. The fin rays have two halves, called hemitrichs, which can slide relative to each other like the halves of a bilaminar strip (Fig. 4). The hemitrichs are made of bony segments which are connected by collagen fibers [11], [21]. The mechanical properties of the fin rays were quantified by conducting three point and cantilever bending tests on individual fin rays and by measuring the force

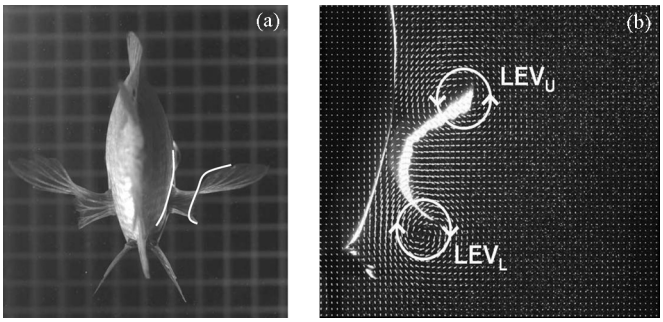

Fig. 5. (a) View from behind the fish, with the cupped pectoral fins moving away from the body. (b) DPIV image representing the sections of the fish shown by white lines in (a). The DPIV data show two large simultaneous leading edge vortices (LEV) on the upper and lower leading edges of the cupped fin.

and displacement that occurred at the ray tip as a result of force and displacement applied at the fin base. The modulus of elasticity for the composite fin ray structure, in all areas, was on the order of 1.0×10^9 Pa, and varied by as much as 12 times between the tip and base of a fin ray. This value is similar to that of human tendons, and reflects that collagen fibers, which connect the segments within each hemitrich, are the mechanism that resists the bending of the fin ray. Flexural stiffness, which is the modulus of elasticity times the area moment of inertia, varied by up to 7.5 times along a ray, with the distal end being less stiff than the base of the fin ray, and by up to 32 times between rays. Representative results for the flexural stiffness of a fin ray near the middle of the fin were 3.2×10^{-6}N m^2 proximally and 0.1×10^{-6}N m^2 distally. The measurements of the force input at the base to output at the tip revealed a 30 : 1 ratio, which reflects that the primary role of the fin rays is that of a displacement transducer. Small displacements at the base lead to large displacements at the tip.

The stress–strain characteristics of the fin's membrane were determined by conducting uniaxial tensile tests on sections of the membrane with dimensions of approximately $2.0 \times 0.5 \times 0.025$ mm^3 that were removed from between adjacent fin rays. The stress–strain curve for the webbing exhibited a "J" shaped curve similar to that of other bioviscoelastic materials with a modulus of elasticity that ranged from approximately 0.15×10^9 to 1.10×10^9Pa.

C. Hydrodynamics

The hydrodynamics of the pectoral fin were studied experimentally using stereo digital particle image velocimetry (DPIV) [22]. The DPIV data demonstrated that during steady propulsion two simultaneous vortices were created along the upper and lower leading edges as the fin moved away from the fish body (Fig. 5). The pectoral fin assumed a cupped conformation, and the active lateral movement of the upper and lower fin edges produced a distinct pair of attached vortices, with the upper vortex being of greater strength than the lower. During maneuvering, the data showed that the lower leading edge can move away from the body before the upper leading edge, and generate a much stronger vorticity early in the fin beat than the upper edge. This was typically seen during maneuvers by the fish where the fin was moved to cause the center of mass of the fish to move downward.

High-fidelity numerical simulations of the pectoral fin of a sunfish in steady forward motion were used to examine key hydrodynamic features and the thrust performance of the pectoral fin. Fin motions digitized from the high-speed recordings were used for the simulations. The computer modeling employs a recently developed Cartesian-grid-based immersed boundary solver that performs both direct numerical simulations (DNS) and large eddy simulations (LES) of flow past highly deformable solid bodies and membrane-like structures as in the fish fin [23]–[26]. Comprehensive experimental and numerical studies were carried out to validate the accuracy of the methods and demonstrated that the results of the simulation were independent of the resolution of the grid and the size of the domain [27], [28].

The CFD simulations matched most of the key topological features seen in the DPIV even though the kinematic data that was analyzed with the CFD were not measured simultaneously with the DPIV measurements. The CFD simulations showed that a complex system of vortices was generated by the fin as it moved through a complete fin beat cycle. Consistent with the DPIV, the simulation predicted the development of a strong tip vortex and leading edge vortices created by the upper and lower leading edges of the fin during both the outstroke from the body and the return of the fin to the body (instroke). This supported the experimental observations that the cupping motion rapidly accelerates the upper and lower edges of the fin and causes the formation of two tip vortices, with the upper being stronger than the lower. The CFD simulations also provided a clear view of the evolution of the vortex structures in the wake.

The hydrodynamic forces produced by the fin were estimated using CFD analysis. Thrust, lift, and spanwise force coefficients are shown in Fig. 6. Note that the positive thrust is produced during all phases of the fin beat, peaks of thrust occur during both fin abduction and adduction, and at no time does the fin produce a net drag force. The existence of the two positive thrust peaks was verified by calculating the acceleration of the fish from high-resolution videos of the fish's movement and by using DPIV data to calculate the force produced by the fin from the change in the momentum of the flow past the fish. This behavior is very different from that observed for canonical rigid flapping foils where drag is usually produced during some phases of the fin beat cycle [18], [25], [29], [30]. The peak magnitudes of the transverse components (lift and spanwise force) are comparable and even somewhat smaller than the peak thrust force. This was unexpected since existing data on flapping foils show that the peak thrust is significantly smaller than the lift force [18], [25], [29], [31], [32]. This is significant in that it implies that this fin motion produces low parasitic forces translating into higher efficiencies, lower bending moments on the fin, and smaller body oscillations. The mean values of these force components over one cycle of fin motion are also small, 0.24 for the lift coefficient and -0.19 for the spanwise force coefficient, as compared to 1.29 for the thrust coefficient. The low mean transverse forces are indicative of the exquisite station-keeping ability of these animals.

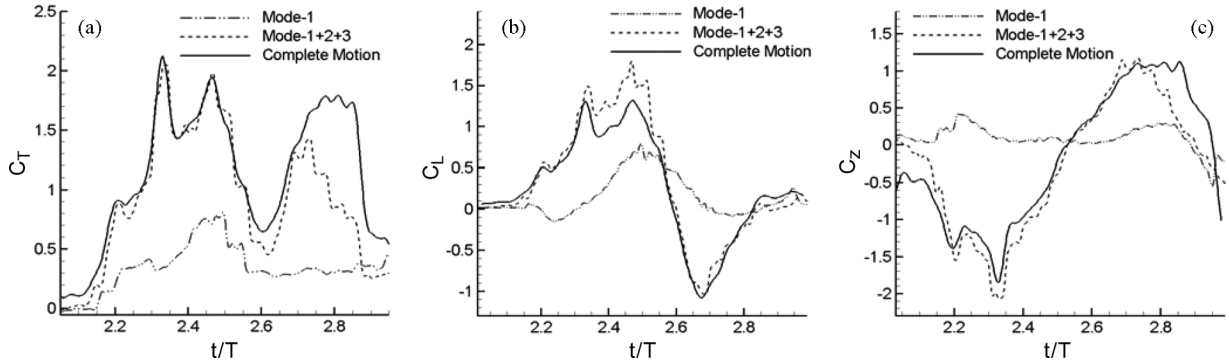

Fig. 6. The coefficients of (a) thrust, (b) lift, and (c) spanwise force predicted for the pectoral fin using CFD. Results for the fin's complete motion (solid) and for POD mode 1 (long dashed), and POD modes $1 + 2 + 3$ (dotted).

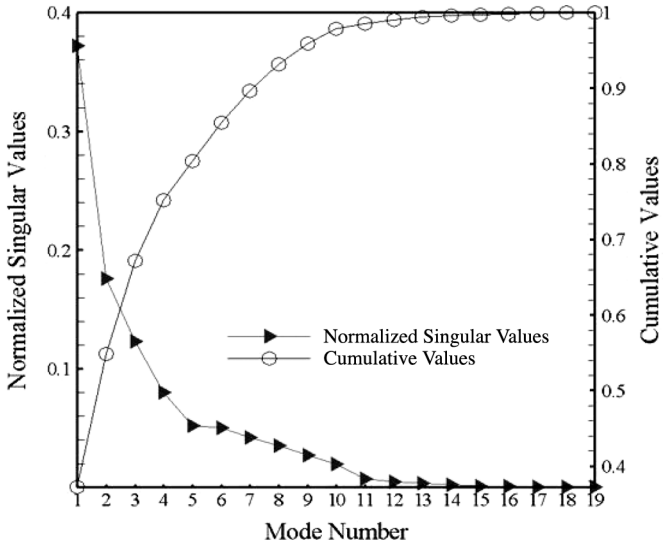

Fig. 7. Normalized singular and cumulative values for the 19 orthogonal POD modes that comprise the pectoral fin's complete motion.

D. Low-Dimensional Models of Pectoral Fin Kinematics

The kinematics of the sunfish pectoral fin were highly complex and did not lend themselves easily to an analysis based on flapping/rowing/paddling kinematics or lift/drag-based propulsive mechanisms. Instead, a more general framework was needed to extract essential features of the fin's gait and to make an intuitive connection between the fin's movements and its hydrodynamics. Proper orthogonal decomposition (POD) [33] was employed to describe the dominant dynamics of the system. It decomposes the motion of a system into orthogonal components that can be studied individually and recombined to reproduce the complete motion of the fin. In this analysis, a full cycle of the fin's motion was described by 20 distinct time frames, and at every time frame the surface data was represented using 280 nodal points in 3-D space. The displacement of every node at each of the time frames was inserted into a matrix and subjected to a singular value decomposition (SVD) analysis which decomposed the fin beat into 19 distinct modes. The singular value spectrum for the fin kinematics is shown in Fig. 7 along with a cumulative plot for the same data. The modes were normalized by the sum of all modes.

The gaits extracted by the POD analysis were then subjected to CFD analysis. Of the 19 modes, we focused on the first three, because together they accounted for over 67% of the variance in the fin's total motion and were highly distinct and relatively easy to interpret. Mode 1 was a "cup and sweep" motion where the fin cups forward about its spanwise axis as it sweeps away (abducts) from the fish's body (Fig. 3). This mode leads to a rapid acceleration of the upper and lower leading edges. An estimate of the forces produced by Mode 1 showed that this cupping motion is instrumental in the production of positive thrust as the fin sweeps forward during the outstroke (Fig. 6). Mode 2 was a "rotation and expansion" where the fin rotates at the base by a few degrees during the outstroke and then expands to present a larger surface area during the instroke. Mode 3 was a rapid "flick" of the spanwise tip of the fin [28]. CFD simulations of gaits made by combining Modes 1 and 2 and Modes 1, 2, and 3 were also carried out. The simulation results showed that a fin motion made by combining these first three orthogonal modes would generate 92% of the thrust produced by the fin's complete motion.

Despite the complexity of the movements exhibited by the sunfish pectoral fin, the POD analysis indicated that it is likely unnecessary for the biorobotic fin to replicate the entire fin motion. The CFD simulations indicated that the cupping of the leading edges as the fin moved away from the fish body was instrumental in producing thrust during the fin's outstroke, and that a majority of the thrust produced by the pectoral fin could be made using motions captured in the first few POD modes.

III. Design of the Biorobotic Fin

A. Design Requirements

Requirements established for the biorobotic fin's design and function were based on the results of the biological studies and on the understanding that the fin's motion and its ability to produce thrust could be approximated sufficiently using a small number of simple component motions. The biorobotic fin must have two leading edges that could be controlled independently. This was important for the formation and control of leading edge vortices and for creating the cupped shape of the fin. The fin must be flexible so that its area could increase during the fin's instroke and so that the effects of the dynamic interaction between

the fin's structure and the fluid could be explored and exploited. Like the fin of the sunfish, the flexibility of the biorobotic fin should increase from the base to the distal end and the base should allow for a small amount of reorientation. In addition to being flexible, the fin should incorporate fin-ray-like structures that would provide active control over the stiffness and curvature of the webbing [21].

Based on the aforementioned requirements, and on the motions described in the first three POD modes, four component motions were defined for the biorobotic fin to be able to perform and to combine to create complex swimming and maneuvering strokes. The most basic motion is a sweeping of the fin away from the body and into the flow (outstroke, abduction) and then back to the body (instroke, adduction). This movement establishes the fundamental fin beat onto which the other component motions are added. The second motion is a cupping of the fin's dorsal and ventral leading edges towards the fin's midline. The third motion is an expansion of the fin in the plane of the fin to increase the surface area. The final motion is a curl about the fin's chord by bending the distal end towards the fin base. This curl can be used to change the curvature and the stiffness of the fin.

B. Fin Design

The basic design of the biorobotic fin consists of several fin rays embedded in a thin urethane webbing (Fig. 2). The bases of the fin rays are attached to a compliant base mechanism that serves as a hinge and the structural support for the fin rays. The base mechanism is clamped into a rigid foundation plate that is attached to an array of servomotors (model HS645MG, Hitec RCD USA, Inc., Poway, CA). The servomotors actuate each of the fin rays individually via nylon "tendons" (Gel spun 35-lb test, The Orvis Company, Inc., Manchester, VT) that attach to the bases of each fin ray and that are guided through passages in the foundation plate.

The webbing was designed as a pleated membrane with a shape similar to that of the biological fin. Pleats are incorporated into the membrane so that the webbing can be expanded to increase the fin's surface area. The linear dimensions of the webbing are approximately three times that of a sunfish pectoral fin, and when the fin is expanded its area increases by approximately 20%. Flat and wavy webbings were tried in addition to the pleated design. Although very flexible and capable of high strains, the flat webs were too stiff to be stretched easily by the fin rays. The wavy webs looked more natural than the square pleats, but did not create as large an area change when expanded. To investigate how webbing stiffness affected the controllability of the fin and its ability to produce force, webs were cast using several urethanes (VytaFlex 10, VytaFlex20, and Evergreen 10; Smooth-On Inc., Easton, PA) with elastic moduli that ranged from approximately 0.10 to 0.15 MPa.

The fin rays (Figs. 2 and 4) serve as the fin's structural members and allow the fin's surface to be actively curved and its stiffness modulated. The top half to one third of each fin ray is a single element, with a notched profile and rectangular cross section that at its maximum is approximately 3.0×0.5 mm^2. The lower portion of each fin ray is split into two halves (hemitrichs), each with a rectangular cross section of approximately 4.0×0.5 mm^2. The lengths of the fin rays range from 85 to 135 mm. The longest ray supports the fin's dorsal edge and the smallest supports the ventral edge. At the bottom of the hemitrichs are the fin ray bases which allow the fin rays to be seated onto the compliant base mechanism. The fin ray bases are kept in contact with the base mechanism by tendons tied to holes in the bases. Like that for fin rays in teleost fishes [21], the curvature and stiffness of the fin rays can be controlled by displacing one of the bases relative to the other and sliding the two hemitrichs past one another (Fig. 4). Copper bands are used to keep the hemitrichs from bowing outward when the fin ray bases are displaced. The bands serve a similar role to the transverse fibers that connect opposite hemisegments in fish fin rays [21]. The fin rays were manufactured using a 3-D stereolithography printer (Viper Si2, 3D Systems Corporation, Rock Hill, SC), and were made from an ultraviolet cured resin (Accura SI 40 Nd, 3D Systems Corporation, Rock Hill, SC), which when cured had approximately a tensile strength of 74.0 MPa and a modulus of elasticity of 3.0 GPa.

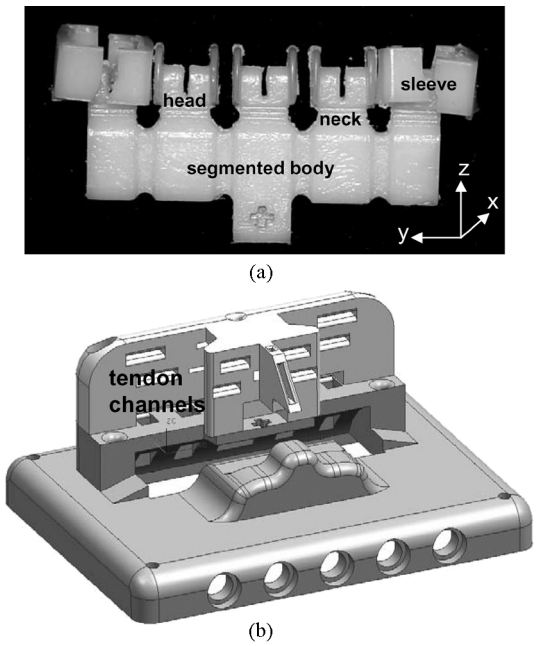

Fig. 8. (a) Compliant base mechanism and (b) rigid foundation plate. The base fits into the foundation plate so that the cross on each piece is aligned. The rectangular channels in the rigid foundation plate serve as passages for the tendons that connect the fin ray bases to the servomotors.

The complaint base mechanism and rigid foundation plate (Fig. 8) serve a similar role as the fibrous cartilage pad, radial bones, and scapula of the sunfish pectoral fin [11]—they support the fin rays and serve as a joint about which the fin rays are moved. The use of a compliant structure, rather than a rigid hinged mechanism with defined planes of motion, allowed for the fin rays to be supported, to have many degrees of freedom, and for the component motions (sweep, curl, cupping, and expansion) to be effectively uncoupled without needing a particularly complex design. The base mechanism comprises the head and neck elements attached to a segmented body. The head supports the fin ray's two bases, and allows each base to be displaced so that the curvature of the fin ray can be controlled.

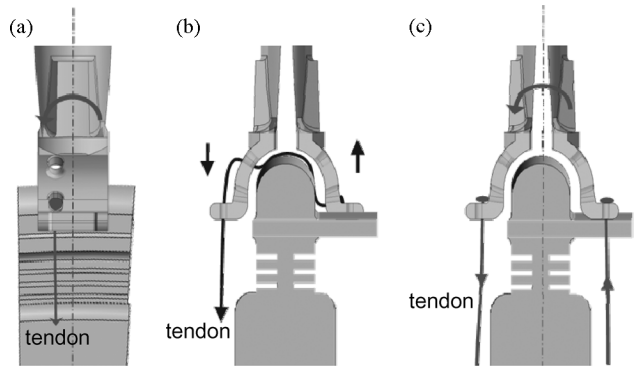

Fig. 9. Tendon actuation. This schematic illustrates how the tendons act upon the fin ray bases to produce (a) expansion, (b) curl, and (c) sweep. The smaller arrows represent directions of motion.

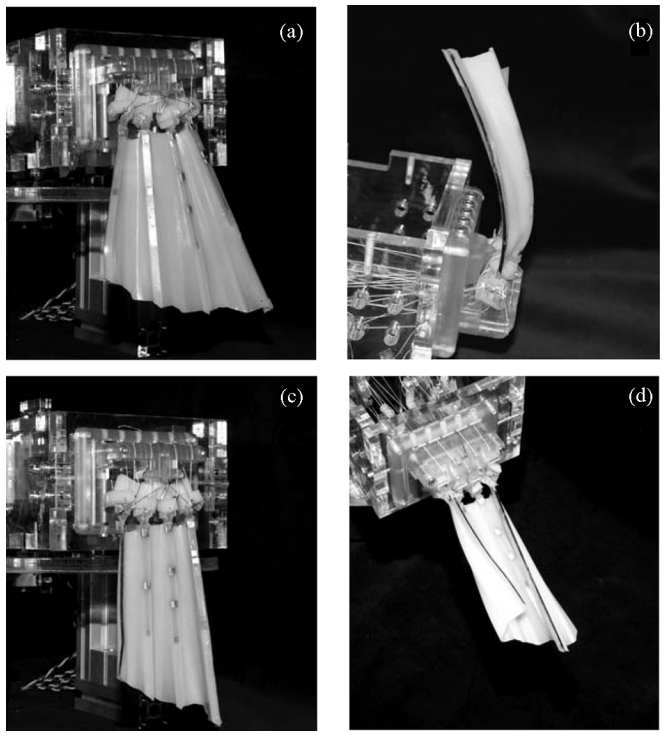

Fig. 10. Component motions: (a) expansion, (b) curl, (c) relaxed, and (d) cupping. Black lines were drawn on the lateral edges of the fin to aid in the visualization of the fin's shape.

Small, vertical sleeves on the sides of each head help prevent the fin rays from being pulled laterally off the heads. The neck elements are designed to bend primarily about the Y-axis, which is defined as the axis that runs laterally through the base. Bending about this axis sweeps the fin rays back and forth, which simulates the adduction and abduction of the sunfish fin. The necks are attached to the segmented body, which is designed to flex primarily about the vertical Z-axis along thin sections that connect each of the body segments. The bending of the segmented body around the Z-axis causes the fin to cup about its span. This is similar to the radial bones in the sunfish pectoral fin which resist Z-direction forces, but can be rotated and shifted in position. The segmented body and necks can also be flexed about the X-axis, which runs horizontally in and out of the base. This motion causes the fin rays to either spread apart or get closer, and enlarges or reduces the surface area of the fin. The compliant base mechanism was cast in a urethane with a tensile strength of approximately 6.1 MPa and an average modulus of elasticity of approximately 1.2 MPa (VytaFlex 60, Smooth-On Inc., Easton, PA). The foundation plate and the molds for the compliant base were designed using computer-aided design (Solid Edge, UGS Corporation, Plano, TX), and manufactured using 3-D stereolithography.

C. Actuation of Component Motions

The tendon's attachment to the fin ray base and the direction that the tendon pulled on the fin ray were critical to producing the four component motions (Figs. 9 and 10). The directions of the lines of force through which the tendons acted were dictated by the location of the tendon's attachment point(s) and the positioning of the passages in the foundation plate through which the tendons passed. Small changes in how a tendon pulled on the fin ray base had a significant impact on how well a motion was actuated.

The sweep of each fin ray was actuated via two tendons, one attached to each half of the fin ray's base [Fig. 9(c)] and driven by a single servomotor. The fin rays were swept forward simply by pulling the tendon connected to the forward-facing ray base and swept back by pulling on the rear-facing ray base. The arrangement is analogous to an agonist/antagonist pair of tendons, with the exception that the tendons were connected to a single motor that could pull in both directions, rather than requiring individual muscles to activate each direction.

To expand the fin, tendons were attached to the fin ray bases, lateral to each ray's midline [Figs. 9(a) and 10(a)]. When pulled, the tendons caused the fin rays to rotate outward and the base mechanism to bend about the local X-axis. One servomotor was used to expand the entire fin.

The curl of each fin ray was also activated using two tendon attachments and a single motor; however, the attachment to the fin ray base was made so that the primary action was to move two halves of the fin ray base relative to each other, rather than to pull the fin ray forward or back [Figs. 9(b) and 10(b)]. Each curl tendon was attached to both halves of the fin ray base. When put in tension, the two halves of the base were first pulled towards each other and held tightly against the head of the compliant base mechanism. This increased the stiffness of the fin ray by preventing either half of the base from moving freely. Further tightening of the curl tendon could cause the fin ray to be pulled forward, as in a sweep motion, but this movement could be prevented by opposing the motion with the appropriate sweep tendon. When the movement was held in check, the curl tendon could be pulled so that the front hemitrich was pulled down, the back hemitrich pulled up, and the fin ray curved forward. The sweep and curl motors had to be operated synchronously to maintain curl in a fin ray as the ray was swept forward.

Several other arrangements for the actuation of sweep and curl were tried in other versions of the fin. The most intuitive arrangement had tendons arranged as an agonist/antagonist pair, one attached to each side of the fin ray. Curl was produced by shifting one tendon relative to the other and sweep was produced

by moving the tendons synchronously. However, this arrangement tended to cause the neck of the base mechanism to collapse, as the lines of force were more downward than forward.

Cupping was actuated independently for the dorsal and ventral halves of the fin using two servomotors. Tendons were attached to the rear base of the dorsal and ventral fin rays to a hole that was lateral to the fin ray's midline. The tendons were drawn forward and into a passage at the centerline of the foundation plate. When pulled, the tendons caused the dorsal and ventral fin rays to rotate and twist the sides of the fin forward, and then to move forward and medially until they touched at the fin midline [Fig. 10(d)].

IV. Experimentation

Four versions of the biorobotic fin were constructed and evaluated to assess their ability to produce the four component motions, and to understand how each of the component motions contributed to the production of thrust and drag. The design, shape, and size of each prototype fin were very similar. The baseline prototype had five fin rays and had its webbing cast from VytaFlex 10. A second version used the same materials and construction, but had only four fin rays. This was done to increase the flexibility of the fin by increasing the amount of webbing between fin rays, and to investigate if the cupping motion could be improved by reducing the congestion of tendons, fin ray bases, and head and neck components at the base of the fin. In the third version, the passive stiffness of the fin was reduced by decreasing the thickness of each fin ray hemitrich and by reducing the length of the two halves before they merged into the single element at fin ray's distal end. The fourth version of the fin used a stiffer urethane (VytaFlex 20) for the webbing material and was used to investigate the effect of webbing compliance.

Each fin and actuator assembly was attached to a carriage that was mounted to the top of a rectangular water tank (Fig. 2). When on the carriage, the fin could be positioned through $+/-60^\circ$ pitch and 360° yaw and be lowered into the tank so that it was submerged completely. The carriage rested on precision air bushings (New Way S301301, New Way Air Bearings, Aston, PA), and could either translate fore and aft or be fixed against an s-beam load cell (Futek L2357, Futek Advanced Senor Technology, Irvine, CA) so that the force produced by the fin could be measured. The arrangement of the biorobotic fin in the tank can be imagined to represent a fish swimming on its side near the water's surface. During the outstroke portion of the fin beat, the fin moves away from the fish's body until it extends into the water and points towards the floor of the tank. During the instroke, the fin is brought back towards the surface until it lies horizontally against the fish body.

The force produced by the biorobotic fin along the X-axis (fore and aft) was measured as the fin was cycled between approximately 0° (horizontal) and 90° (vertical). The fin's movements were created using a basic sweep motion, and then by adding combinations of curl, expansion, and cupping to sweep. Simple sinusoids were used to drive the sweep, curl, and expansion motions at 0.60 Hz. This frequency is approximately one third the flapping frequency used by the sunfish, and was selected so that the robotic fin, which is approximately three times the length of a sunfish fin, would have a Strouhal number similar to that of the sunfish fin at similar flow rates. Cupping was activated using a square wave. The use of sinusoids, rather than a signal that had a velocity profile shaped to improve thrust and reduce drag, made it easier to compare the effect that different fin conformations had on thrust. Since the commanded velocity was the same on the outstroke and instroke, changes in force were related directly to changes in the fin's shape and its effect on the water. All tests were conducted without a free-stream current in the tank.

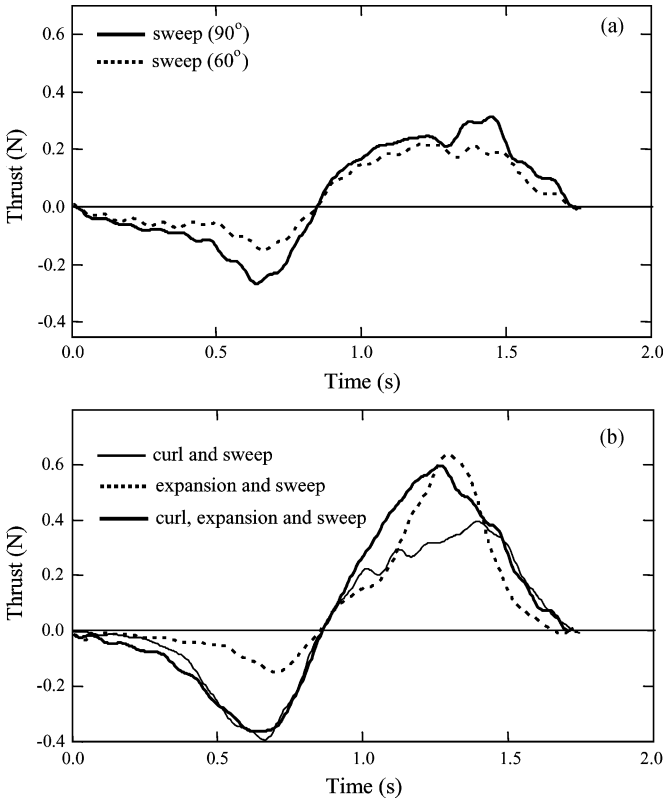

Fig. 11. Forces created by the baseline, five-ray fin. (a) Force created by the fin using the sweep motion when the fin was cycled through 90° from the horizontal to the vertical (solid), and through 60° centered about 45° (dashed). (b) Force created by the fin using a 60° sweep plus: curl (thin solid), expansion (dashed), and both curl and expansion (thick solid). A summary of the forces and impulses for the baseline fin is shown in Table I, in the rows labeled fin A.

Data were collected at 200 Hz using a National Instruments 6062-E data acquisition board (National Instruments Corporation, Austin, TX). Representative results for the force produced during a single stroke cycle (instroke, outstroke) were made by averaging the force in five stroke cycles, and then by lowpass filtering the averaged result at 10 Hz. The lowpass filter was designed using the Kaiser window method to have a passband frequency of 10 Hz, a stopband frequency of 12 Hz, and a peak error of 10^{-4} [34]. The data were processed using applications written in Mathcad 11 (Mathsoft Corporation, Cambridge, MA).

The effectiveness of the fin at producing thrust was evaluated by calculating the impulse imparted on the water by the fin in the X-direction. The impulse, which equals the change in momentum of the water, was approximated using $I = \sum_j F_j \Delta t$, where I is the net impulse, Δt is the sampling period, and F_j is the force created by the fin in the X-direction sampled at time $j \times \Delta t$.

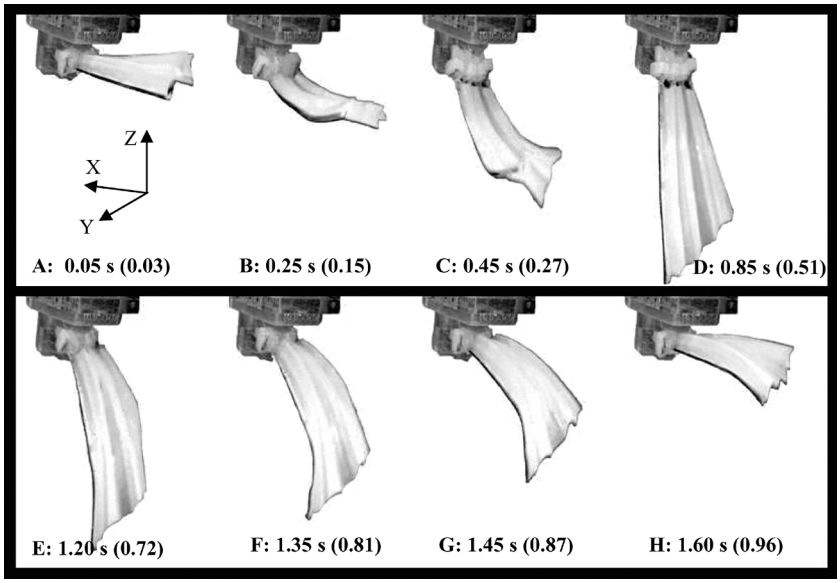

Fig. 12. Images from a video of the four-ray fin conducting a simple sweep motion. The camera angle was from approximately 45° aft of the Y-axis. The outstroke is shown in panels A–D, and the instroke in panels E–F. The main plane of the fin was aligned predominantly with the Y-axis during sweep. The time stamp indicates the time within the 1.67-s cycle and the number in parenthesis represents the decimal fraction within the fin's cycle.

V. Results

A. Sweep

The data displayed in Fig. 11(a) are typical of the forces produced by the fin when the fin was moved using the sweep motion (Fig. 12). The curve with the larger amplitudes (solid) represents the thrust (positive force) and drag (negative force) produced when the fin was cycled through a full 90° displacement. The smaller amplitude curve (dashed) represents the force produced by the fin when the fin was cycled through approximately 60°. Because coupling between the curl and the sweep component motions would cause the fin to be displaced through a greater angle than when the fin was moved by sweep alone, it was necessary to reduce the magnitude of the sweep component when it was combined with the curl component to maintain a 90° displacement. Therefore, the 60° sweep motion is what was built upon when other components were added to the sweep motion, but it is the force produced during the 90° displacement that was compared directly to the force produced by other fin motions that moved through 90°.

All versions of the biorobotic fin produced a larger magnitude peak thrust during the fin's instroke than peak drag during the outstroke. The periods over which thrust and drag were produced were nearly equal. The result was that the fins were able to impart a net positive impulse on the water using only the sweep motion, which would act to propel a UUV forward. In the example shown in Fig. 11(a), which is from the baseline prototype, the maximum thrust during the 90° displacement was 0.33 N and the maximum drag was -0.28 N. The change in momentum created by the fin's thrust was 0.17 kg m s^{-1}, which was 70% greater than the -10 kg m s^{-1} change in momentum created by the fin's drag.

All fin versions performed similarly when the amplitude of the sweep displacement was reduced from 90° to 60°, but as expected, the force and impulse exerted on the water was decreased. The shapes of the force curves were similar, but the maximum thrust and drag were reduced by 30%–40%, as was the net momentum imparted to the water. In the example shown in Fig. 11(a), maximum thrust decreased from 0.33 to 0.21 N, the magnitude of the peak drag decreased from 0.28 to 0.17 N, and the net change in momentum decreased from 0.07 to 0.05 kg m s^{-1}.

When moved through the water using only sweep, the fins did not appear to be very rigid. The fins would bend along their length, from the base to the tip of the fin rays, away from the direction of movement (Fig. 12). Although the biorobotic fins were very flexible, they did not appear to be nearly as compliant as the sunfish pectoral fin. Whereas the biological pectoral fin has a fluidity to its movement, the biorobotic fins moved more stiffly. Decreasing the number of fin rays from five to four, which made the fin more compliant by increasing the amount of webbing material relative to the number of structural supports, caused the biorobotic fin's motions to look smoother, less mechanical, and consequently more biological.

B. Curl and Sweep

Curl was designed to affect the curvature and stiffness of the fin, but it was not decoupled completely from the sweep movement. When activated, it caused the fin to curve [Fig. 10(b)], but also to be rotated forward or back, and when added to a sweep movement would cause the fin to move through a greater displacement. Therefore, the amplitude of the curl motion was selected so that when added to a 60° sweep, the fin would move through 90°. Curl could be used to affect stiffness or the shape of the fin without rotating the fin by using the sweep actuators to oppose the motion induced by the curl component motion. This worked well when the fin was held statically, but became more difficult to accomplish when the fin was being swept to produce force.

Compared to a 90° sweep movement, the combined curl and sweep motion increased both the magnitude of the peak thrust and drag and the impulse imparted to the water. But because the

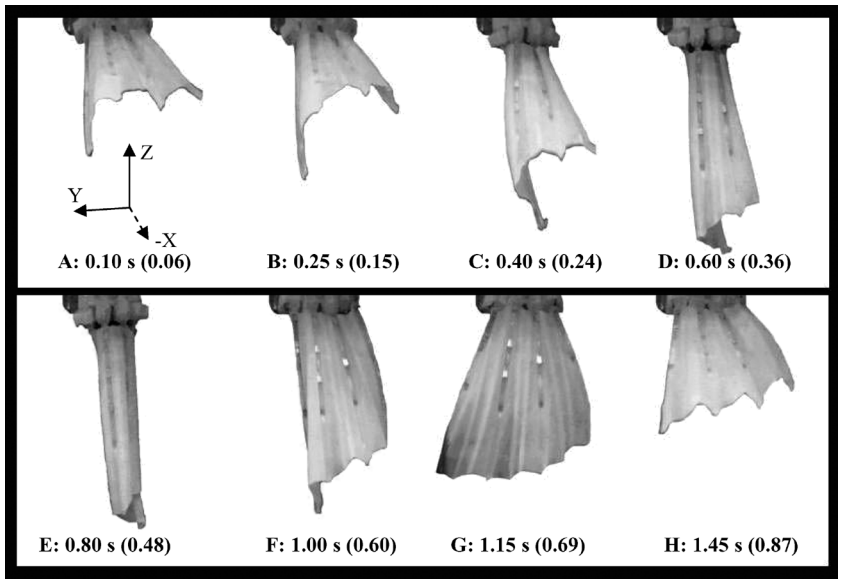

Fig. 13. Images of the four-ray fin conducting a motion that combined all four components: sweep, curl, cupping, and expansion. The camera angle was from approximately 85° aft of the Y-axis. The fin cupped about its spanwise axis as it swept forward (panels A–D), formed almost a cylinder as it transitioned from the outstroke to the instroke (panel E), and then uncupped and expanded during the instroke (panels F–H). The curl component did not alter the shape of the fin significantly, but did serve to stiffen the fin. This sequence demonstrates the most extreme cupping motion that the robotic fins were able to execute. Like for the fish, the dorsal (left) edge is cupped farther forward than the shorter, ventral edge. However, in this case, the dorsal edge was pulled far forward, past the midline of the fin, such that the backside of the fin was presented to the oncoming flow. During trials conducted to measure force, the maximum amount of cupping was limited to be like that shown in panel C.

impulse was increased during both the thrust and drag portions of the stroke cycle, the net momentum imparted to the water by the fin when curl and sweep were combined was not significantly greater than when sweep alone was used. In the example shown in Fig. 11, the maximum thrust increased from 0.33 to 0.39 N and the impulse created by the thrust increased from 0.17 to 0.20 kg m s^{-1}. The magnitude of the peak drag increased from 0.27 to 0.41 N and the drag impulse increased from 0.10 to 0.13 kg m s^{-1}. The net impulse of 0.07 kg m s^{-1} was identical to the net change in the momentum from sweep alone.

Visually, the fin appeared more rigid than when moved through the water by sweep alone. The distal end of the fin still bent away from the direction of motion, but overall there was much less of a bend in the fin from the base towards its distal end.

C. Expansion and Sweep

The addition of expansion to the instroke of the 60° sweep motion had a significant effect on the thrust and impulse produced by the fins [Fig. 11(b)]. In general, the peak thrust more than doubled, while the drag force created during the outstroke was largely unchanged. The result of greatly increasing the fin's thrust, but not significantly its drag, was that the net positive impulse imparted to the water by the fin was greatly increased by the addition of the expansion component. In the example shown in Fig. 11, adding expansion to the 60° sweep motion increased peak thrust from 0.21 to 0.62 N, while the magnitude of the maximum drag increased only from 0.17 to 0.18 N. The impulse from the thrust force was 0.20 kg m s^{-1} and from the drag force was -0.08 kg m s^{-1}. The net change in the momentum of 12 kg m s^{-1} was more than double that from the 60° sweep motion alone.

Because expansion was activated using a sinusoid, the fin's area was not increased equally through the entire instroke and, therefore, the thrust was not improved uniformly. As can be seen in Fig. 11, the thrust produced using the expansion and sweep components began the same as when sweep alone was activated, but rose to a much larger value and dropped more quickly. The timing of the peak in the thrust was controlled by the phase relationship between the expansion and sweep sinusoids. Expansion of the fin is shown in Fig. 13, although the motion is complicated slightly in these images by the fin uncupping at the beginning of the instroke.

D. Curl, Expansion, and Sweep

Adding both expansion and curl to the sweep motion elicited both the benefits and drawbacks of both component motions. In general, the maximum thrust was as large as when the fin was moved using expansion and sweep, and the duration over which a larger magnitude of thrust was produced was as long as when curl and sweep were used [Fig. 11(b)]. This resulted in the impulse that was imparted to the water by the thrust to be larger than when either curl or expansion was combined alone with sweep. The drawback to this combination of components was that the drag force and the impulse imparted to the water by the drag was also large. As can be seen in Fig. 11, the drag force was almost identical to the force produced by the fin when curl and sweep were used. This large drag force effectively negated the benefit of the large and long-duration thrust. In three of the four biorobotic fins, the net impulse produced using curl, expansion, and sweep was greater than when sweep and curl were used, but less than when expansion and sweep were used. The net impulse from expansion, curl, and sweep was 0.10, 0.12 kg m s^{-1} from expansion and sweep and 0.07 kg m s^{-1} from curl and sweep.

E. Cupping, Curl, Expansion, and Sweep

Cupping was initiated at the beginning of the outstroke [Fig. 13(a)] and was maintained such that the fin was cupped about its span-axis as it was swept from the horizontal to the vertical. The cupping component pulled the ventral and dorsal fin rays forward of the medial section of the fin so that two leading edges were created during the outstroke [Fig. 13(b)]. As the fin was swept forward, a pocket formed in the medial section such that the fin's shape was somewhat cylindrical. Cupping was turned off at the beginning of the instroke so that the fin's area could be increased by the expansion component [Fig. 13(g)].

This fin motion, which combined all four component motions, was similar to that of the sunfish during steady swimming, especially during the first half of the outstroke [Fig. 13(a)–(c)] and the second two thirds of the instroke [Fig. 13(f)–(h)]. A DPIV analysis of the flow around the fin showed that, like the sunfish fin, cupping of the robotic fin's upper and lower leading edges produced vortices on the fin's upper and lower surfaces. Although the movement and conformations of the biorobotic and sunfish fins were similar, there were obvious differences between the motions. First, the biorobotic fins were swept through 90°, from the horizontal (0°) to the vertical (90°). This was greater than the approximately 45°–65° through which the sunfish fins are typically swept, but was selected as the standard because it was convenient for experimentation. A second difference was in the amount that the fins bent as they moved through the water. As shown in Fig. 3, the upper and most spanwise portions of the sunfish fin were bent away from the direction of the fin's movement. The biorobotic fins exhibited a similar amount of bending when swept through the water without the cupping component (Fig. 12), but the amount of bending was reduced when the cupping component was added to the sweep motions.

Representative results are shown in Fig. 14 to illustrate the effect that cupping had on the force produced by the fin. The drag force produced by the fin changed significantly when cupping was used. The maximum magnitude of the drag force was always reduced, sometimes by half. However, this did not always cause the impulse from the drag force to be lowered. The timing and shape of the drag profile were also affected, which caused to increase the impulse created by the fin's drag force in some trials and to decrease the impulse in others. In the example shown in Fig. 14, the addition of cupping caused the magnitude of the peak drag force to decrease from 0.50 to 0.39 N, but the impulse from the drag remained -0.17 kg m s^{-1} due to the greater duration over which drag was produced.

Cupping, which was deactivated near the beginning of the fin's instroke, had little effect on the thrust. The timing of when the thrust force peaked and its duration were slightly different from when cupping was not used, but the values of peak thrust and its total impulse changed very little. In the example shown in Fig. 14, peak thrust dropped from 0.60 to 0.58 N, and the impulse from the thrust decreased from 0.26 to 0.24 kg m s^{-1}.

F. Cupping Alone

To see the effect of cupping alone, the fin was held in the horizontal position and the cupping component was actuated. The magnitudes of the forces were much smaller than those created when the fin was swept forward and back, but interestingly the cupping motion produced two regions of thrust. Similar to the sunfish, positive thrust was generated as the fin was cupped and then again as the fin was uncupped [Fig. 14(b)]. There was little difference in the magnitudes of the forces that were created by each of the four prototype fins.

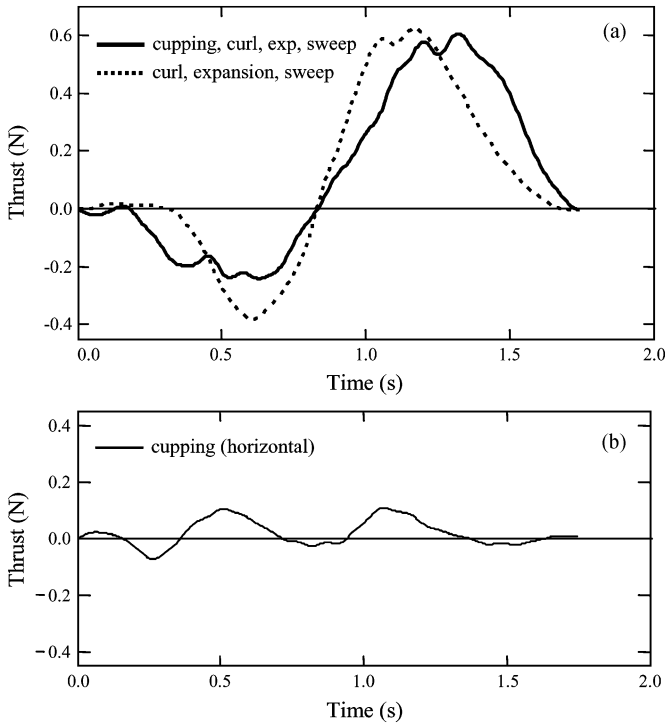

Fig. 14. Effect of cupping on the force produced by the four-ray fin. (a) Force created by the fin using sweep, curl, and expansion (dashed), and when the cupping component was added to sweep, curl, and expansion (solid). (b) Force produced exclusively by the cupping component when the fin was positioned horizontally.

G. Rowing

A motion that resembled rowing, where the fin was feathered into the water during the outstroke and then made to paddle back during the instroke (Fig. 15), was used to determine if the drag force could be lowered significantly while still creating a large thrust using a paddling motion. Trials were conducted with the four-ray fin only. The feathering motion was made by combining asymmetric cupping, sweep, and curl components. The dorsal edge of the fin was cupped and the dorsal fin ray was swept through 90°. The more ventral rays were swept forward actively with reduced displacements. This caused the fin to effectively rotate about the base such that the fin's motion was led by the dorsal edge [Fig. 15(b)–(d)]. The more ventral fin rays lagged behind the dorsal fin ray, but were then pulled forward as the compliant base was stretched.

Visually, the dorsal edge of the fin seemed to move strongly through the water, while the ventral half appeared to follow passively and to be very compliant. The fin, led by the motion of the dorsal edge, would twist smoothly into the flow, and then as the dorsal edge was uncupped and the dorsal ray swept back, the

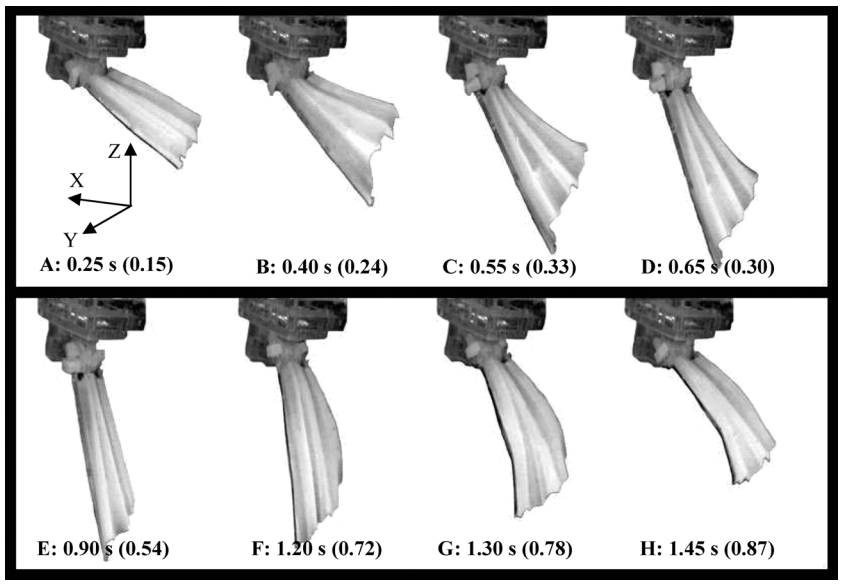

Fig. 15. Four-ray fin conducting a rowing motion. The camera angle is from approximately 45° aft of the Y-axis. The fin was twisted and feathered into the flow such that its motion was led by the fin's dorsal edge (panels 1–4). The fin was then brought square with the flow (panel 5), such that the main plane of the fin was aligned with the Y-axis and all fin rays were paddled back together (panels 6–8).

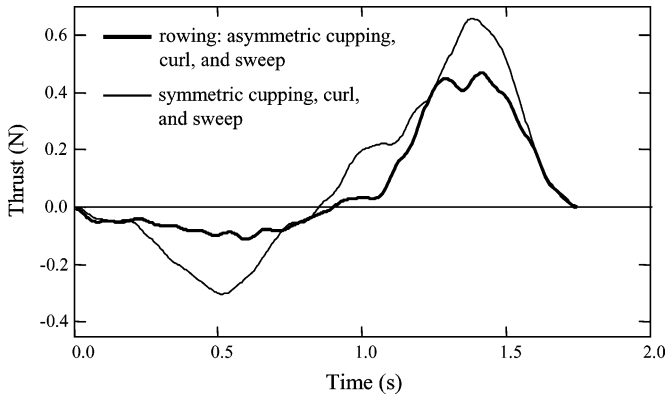

Fig. 16. Forces from the rowing motion. The force created by the fin using sweep, curl, and cupping (thin solid), and when the fin was feathered into the flow during the outstroke by using an asymmetric sweep, curl, and cupping (thick solid).

fin rays would seem to align and complete the last half of the instroke together such that the plane of the fin was perpendicular to the direction of movement [Fig. 15(f)–(h)].

Of all combinations of the component motions, the rowing movement produced the lowest peak drag force and smallest drag impulse. Representative results are shown in Fig. 16. The peak drag produced by the feathering motion was one third of that produced by the normal sweep, curl, and cupping components (-0.12 versus -0.39 N) and the impulse from the drag was about half (-0.06 versus -0.11 kg m s^{-1}). Thrust and its impulse were also reduced. Peak thrust decreased from 0.63 to 0.48 N and its impulse decreased from 0.28 to 0.19 kg m s^{-1}. Although the drag forces were lowered significantly, the net impulse imparted to the water by the fin was smaller than when the fin's motion was not feathered and all fin rays were moved through a full 90° (0.13 versus 0.17 kg m s^{-1}).

H. Decreased Passive Stiffness in Fin Rays

The prototype fin that used fin rays with the lowest passive stiffness generally had lower peak thrust and drag forces, and imparted less impulse to the water during the separate periods over which the thrust and drag forces occurred. A comparison of forces and the impulse created by the forces is shown in Table I for this five-ray fin (fin B) and the baseline, five-ray fin (fin A).

Visually, this fin appeared pliant and was bent further when swept through the water than the baseline fin. Also, the force profiles were more oscillatory and varied more in magnitude than the force produced by the fins that used more rigid fin rays. In contrast to the results for the other fins, the 90° sweep motion created larger peak forces than did the combined curl and sweep motion. However, as with the other fins, the use of curl to actively stiffen the fin rays increased the impulse from the thrust and drag and improved the fin's ability to impart momentum to the water.

Although reducing the passive stiffness of the fin rays decreased the fin's ability to change the momentum of the water with its thrust and drag forces, the net change in the momentum that the fin created was not always smaller than the stiffer fins. In the example shown in Table I, the net impulse for the fin with reduced stiffness was slightly higher than for the fin with the stiffer fin rays when the fins were actuated using sweep, curl, and expansion, and using sweep, curl, expansion, and cupping.

I. Increased Webbing Stiffness

The use of a 50% stiffer webbing material effectively negated the ability of the curl component to modulate the stiffness of the fin and to affect the force produced by the fin. Overall, the performance of this fin was similar to that of the other five-ray fins when they had the curl component activated. The expansion and cupping components affected this fin's performance in the same manner as described for the other fins. However, unlike

TABLE I
COMPARISON OF FORCES AND IMPULSES BETWEEN BASELINE FIN (A) AND FIN WITH FIN RAYS OF LOWER PASSIVE STIFFNESS (B). IN ALMOST ALL CASES, THE STIFFER FIN RAYS RESULTED IN HIGHER FORCES AND IMPULSES (SHOWN IN BOLD)

		Peak force (N)		Impulse (kg m s^{-1})		
motion	fin	thrust	drag	thrust	drag	net
sweep (60^{o})	A	**0.21**	**-0.17**	**0.12**	**-0.07**	**0.05**
	B	0.14	-0.12	0.07	-0.06	0.01
sweep (90^{o})	A	**0.33**	-0.28	**0.17**	-0.10	**0.07**
	B	0.32	**-0.36**	0.12	**-0.11**	0.01
sweep and curl	A	**0.39**	**-0.40**	**0.20**	**-0.13**	**0.07**
	B	0.25	-0.27	0.14	-0.12	0.02
sweep, curl, and expansion	A	**0.60**	**-0.39**	**0.26**	**-0.16**	0.10
	B	0.48	-0.18	0.19	-0.08	**0.11**
sweep, curl, expansion, cup	A	**0.52**	**-0.50**	**0.24**	**-0.17**	0.07
	B	0.39	-0.27	0.20	-0.12	**0.08**

the other fins, there was very little difference in the thrust and drag produced by the fin when curl was activated or deactivated.

VI. DISCUSSION

A. Biorobotic Fin Design

The key to the success of this design as an experimental device and as a prototype UUV propulsor were the high level of control over the fin's motion and shape and the flexibility that existed in how the fin could be used. By actuating individual fin rays with tendons that pulled in several directions, rather than by actuating the fin as a single foil with only a few degrees of freedom, and by having a base and webbing that could be twisted, reoriented, and flexed, few constraints were placed on how the fin could be moved, and an enormous amount of freedom was available to explore how the fin could be manipulated to produce thrust. The fin was able to create the desired four component motions, could be commanded so that the component motions were combined essentially independently, and could be made to produce fin motions not commonly used by the sunfish, such as feathering and paddling. Once this design is made more robust, it will be an excellent candidate for an analysis that discovers, through artificial evolution [35] or other optimization methods, fin motions that are ideal for producing thrust and maneuvering forces. Although the sunfish is very effective at producing and vectoring thrust, motions that replicate the kinematics of the sunfish pectoral fin may not necessarily be optimal for use by a UUV.

However, the biorobotic fin's level of control and many degrees of freedom were a direct result of using a design that was based heavily on the anatomy of the sunfish pectoral fin. The designs of the fin rays, flexible webbing, compliant base mechanism, nylon tendons, and isolated actuators were simple relative to Nature's, but they all retained the basic functionality of their biologic counterparts. The elegant bilaminar design borrowed for the fin rays allowed for the curvature and stiffness of the fin to be actively controlled without requiring actuators or complex linkages to penetrate the fin webbing. The webbing remained thin and the fin very flexible, yet the fin could be shaped and adjusted locally to have desired characteristics. The compliant base mechanism, like the radial bones and cartilage pad in the pectoral fin girdle, gave support, yet allowed the fin to be bent and twisted. The use of such a design, coupled with the detailed knowledge of the sunfish pectoral fin's kinematics and anatomy, made it easier to identify and study fin properties, such as flexibility, that affect motion and force production.

The stiffness of the fin rays and webbing was shown to be important to the production of thrust. The general conclusions are that the webbing should be very flexible so that it can be expanded and contoured by the fin rays, and so that the fin moves smoothly and gracefully through the water, like the fin of the sunfish. For this design, webbing material with a modulus of elasticity of 0.10 MPa was found empirically to work well. When a urethane that was 50% stiffer was used, the fin moved more like a rigid plank than a compliant structure, and any advantages from there being a dynamic interaction between the flexible structure with the fluid may have been lost [18], [36]. The stiffer webbing also prevented the fin rays from being able to actively increase the stiffness of the fin, consequently eliminating their ability to modulate the force produced by the fin. Relative to the webbing, the fin rays should be stiff enough so that the fin moves through the water without bending or flapping excessively, and they must be designed so that their passive stiffness is complemented appropriately by the increase in stiffness that occurs when they are actively curled. As shown by Table I, the stiffness of the fin rays affected the level of force produced by the fin. In general, the fin with stiffer fin rays produced higher levels of force. There was, however, approximately the same increase in thrust and drag when the fin rays were actively stiffened. Additionally, we believe that the dimple that forms on the upper surface of the sunfish fin (Fig. 3) is crucial to the movement of the vortices along the upper fin surface (Fig. 6), and

that its formation is due to the fish modulating the stiffness of the fin in that area. To accomplish this well with the biorobotic fin, the flexibility of the fin will have to be tuned distally as well as chordwise by designing the properties of each fin ray individually.

The webbing of the biorobotic fin was pleated so that the fin's area could be more easily expanded by spreading the fin rays. The webbing of the sunfish pectoral fin does not have large pleats like the artificial web, but pleats are not unheard of in biological wings [37]. The effect that the spanwise pleats have on the hydrodynamics of the biorobotic fin has not yet been determined.

The compliant base mechanism (Fig. 8) allowed for complex fin motions to occur without the need of a complicated hinge structure. It allowed the base of the fin to be bent, rotated, and twisted, and for the fin rays to be moved in their desired directions. Constraints on the motion of the fin rays were imposed only by the direction with which the tendons pulled the base of each ray and by the structure or hydrodynamics resisting a motion with more force than could be exerted by the servomotors. The many degrees of freedom offered by the base mechanism were crucial to being able to mix component motions and to create interesting combinations of movements.

The compliance of the base mechanism did, however, cause some difficulties. In particular, the flexibility of the head and neck structures affected how the curl component could be actuated. Rather than being able to implement curl and sweep in a manner similar to the fish, where a pair of agonist/antagonist muscles is used to displace the two bases of a fin ray relative to the other, curl was implemented using a single tendon that pulled up on one fin ray base and down on the other. When curl was implemented using the agonist/antagonist method, the head and neck of the base mechanism tended to buckle and prevented sweep from being actuated smoothly. By switching to the single tendon method [Fig. 9(b)] the two fin ray bases were first pulled tightly against the head and then were shifted in position. This caused the stiffness of the fin rays to be increased, but also for the fin rays and the fin to be pulled forward. This meant that curl was not decoupled from sweep, but did make it possible to modulate the stiffness of the fin. To account for the movement caused by the curl actuators, the amplitude of the sweep actuators was reduced so that the fin was swept through the same displacement in all experimental trials.

As in the sunfish, where the muscles that act on the pectoral fin are in the fish's body, the actuators for the biorobotic fin were isolated from the fin and transferred forces via tendons. The modularity of this design means that any actuators with appropriate performance specifications can be used. The servomotors used in these first generation prototypes were not ideal, but were selected because of the ease with which they could be implemented and their affordability. Their primary drawback is that they do not offer explicit control over their force output or the velocity at which they move to a commanded position. It was found experimentally that their position could be updated no faster than every 0.06 s (16.67 Hz). This produced satisfactorily smooth 0.60-Hz motions, but limited how quickly the fin could be moved and its position controlled. The next generation prototype will implement linear Lorentz force actuators that will be built inhouse for improved performance.

B. Component Motions and Coupling

The biorobotic fins produced the sweep, curl, expansion, and cupping motions that were good first-order approximations of the motions observed in the first three modes of the POD analysis. These four component motions were combined to produce complex fin motions that looked biological and similar to the movements made by the sunfish pectoral fin.

The four component motions could be combined, but they were not completely decoupled: the activation of curl caused the fin to sweep forward and/or back and the cupping motion interfered with expanding the area of the fin. These interactions meant that a component motion could not be added to a movement without regard for the components that were already being actuated. This coupling of component motions made it slightly more difficult to attribute changes in the forces produced by the fin solely to the phenomenon that an individual component was designed to create. For example, more thrust was produced during the fin's instroke when using expansion, curl, and sweep than when using only curl and sweep [Fig. 11(b)]. The increased peak thrust was due largely to the area of the fin being increased by the expansion component. However, we cannot be certain that all of the force increase was due to the fin's larger area, as the interaction between cupping and expansion may have also caused a change in the shape of the fin's surface. Obvious interactions between component motions were addressed by altering how the components were used and combined. When curl was added to a sweep motion the amplitude of the sweep component was reduced so that the displacement of the fin during the fin beat remained 90°. The coupling between cupping and expansion did not have a great effect on the fin because the two component motions were not actuated simultaneously. Cupping was used during the outstroke and expansion during the instroke. How quickly cupping was deactivated did affect how quickly the expansion component was able to increase the area of the fin.

C. Forces From Component Motions

The sweep, curl, and expansion components affected the forces produced by the fin in a manner that was expected, and provided insight into how these component motions might be combined to produce forces appropriate for propelling and maneuvering a UUV. The basic sweep motion (Fig. 12) produced near-equal periods of thrust and drag, with the magnitude and impulse of the thrust being greater than that of the drag [Fig. 11(a)]. The net impulse imparted to the water was positive, which would tend to propel the UUV forward. This force can be biased more towards thrust, and made more appropriate for use in propelling a UUV, by sweeping the robotic fin from the horizontal through an angle smaller than the 90° used in these studies.

The addition of curl to the sweep motion stiffened the fin by pulling the bases of each hemitrich tightly against the heads of the base mechanism, and increased the magnitude and impulse of the thrust and drag forces. Because curl was activated

during both the instroke and outstroke, thrust and drag were affected similarly and the net impulse the fin imparted to the water was not improved. However, these results demonstrated that the force produced by the fin can be modulated by actively controlling fin stiffness. Without changing the motion of the fin, it is possible to increase or decrease quickly the forces being produced simply by altering fin stiffness. This gives a fine level of control over the force produced by the fin, and could be advantageous during the maneuvering of a UUV, which can require quick and small adjustments to thrust and drag. For an application that wanted to maximize net thrust, it would thus be appropriate to stiffen the fin during the instroke and then reduce the fin's stiffness during the outstroke.

The expansion component increased the area of the fin during the instroke and greatly increased the magnitude of the thrust force. The period over which the thrust was increased was short, but this was due to the expansion component being activated using a sinusoid rather than a signal that expanded the fin fully over a greater duration. The increase and decrease in the thrust corresponded to the rise and fall of the sinusoid. When used to propel an underwater vehicle it would obviously be beneficial to hold the area of the fin open for a longer period.

When the sweep, curl, and expansion component motions were combined, the forces produced were approximately the summation of the forces produced by the individual sweep, curl, and expansion components [Fig. 11(b)]. The increased area and stiffness of the fin during the instroke produced a very good thrust force, but because the curl component was not deactivated during the outstroke, the drag force and its impulse were also large. If used to propel a UUV, it would be more appropriate to activate curl and expansion during the instroke to increase thrust and to decrease drag during the outstroke by deactivating curl and reducing the stiffness of the fin.

The rowing motion demonstrated one manner in which the sweep, curl, and expansion components could be used to create a high force during the instroke and low drag during the outstroke. For this motion, the fin was angled, or feathered, during the outstroke so that the fin moved forward with a single leading edge. The fin was then rotated to a more vertical position, and then paddled back to produce thrust. This movement is effectively aquatic rowing [16]. Although this rowing motion did not produce as great a net impulse as when sweep, curl, and expansion were used without feathering, it did produce the lowest peak drag force and the smallest drag impulse (Fig. 16) of any fin motion that involved the sweep component. This would result in the fin or UUV having a smoother motion through the water because it would not be decelerated as much with each stroke.

This type of motion demonstrates the flexibility of this design and highlights an important difference between this biorobotic fin and more typical implementations of robotic pectoral fins [5], [38], [39]. The many actuators and the flexibility of this biorobotic fin enable it to create motions that potentially span the space that ranges from rowing to flapping [16] to the complex dual leading edge motions of the sunfish. A UUV that employs such a biorobotic fin could, therefore, use whichever motion was most efficient or effective for its speed and behavior.

An important difference between the dual leading edge motion, which is common among many fish, and the rowing and flapping motion, which represent less common but more extreme pectoral fin movements, is the production of drag. At low speeds, the power stroke of a rowing motion is very effective at creating large forces for maneuvering [13], [16]. However, even when the fin is feathered into the flow during the recovery stroke, the fin produces drag which works against the forward motion of the fish and reduces its efficiency. This is not the case for the dual leading edge motion of the sunfish pectoral fin, which can produce positive thrust during all phases of the fin beat. Implementing such a motion could greatly improve the efficiency of fin-based propulsion and maneuver, as the fin will not produce drag that retards forward motion and its small lateral and lift forces are less likely to cause oscillations that can interfere with hovering.

The cupping component was added to the fundamental sweep of the fin to create the dual leading edge motion employed by the sunfish and as a mechanism for producing positive thrust during the outstroke. As with all of the fin motions that employed a sweep of the fin, thrust was produced during the fin's instroke, but the cupping motion did not cause thrust, instead of drag, to be created during the outstroke. This differs from the results for the sunfish and for POD mode 1 where the combination of cupping and sweep was shown to produce thrust as the fin moved away from the fish body. The peak magnitude of the robotic fin's drag force was generally reduced by the cupping motion [Fig. 14(a)], but this is believed to have been due to the cupping movement reducing the area of the fin and putting the fin in a lower drag, cylindrical shape. This is supported also by the increased duration of the drag force profile, which corresponds more closely to the time that the fin is being moved forward.

However, results that show that the cupping component can indeed produce a thrust force during the outstroke were seen when the fin was positioned horizontally and cupping was activated without any sweep. In these trials, two peaks of thrust were created as the fin was cupped and then reopened [Fig. 14(b)]. The magnitude of these thrust peaks was small, about 0.1 N, so if the cupping motion had produced this level of force when the fin was also being swept forward, the thrust would have been masked by the larger drag forces created by the other component motions.

The different relative magnitudes of the cupping and sweep movements in the sunfish and in the biorobotic fin may explain why the thrust from cupping of the biorobotic was too small to overcome the drag force. For the sunfish, the POD analysis identified that the pectoral fin's movement was dominated by the cupping motion. Mode 1, which can be described as cupping with a slight sweep, accounted for 40% of the fin's total movement. Relative to the thrust produced by cupping of the leading edges, the drag produced by the sunfish fin's slight sweep forward was probably small. A POD analysis has not been conducted on the biorobotic fin, but in contrast to the sunfish, the sweep motion of the biorobotic fin moved the fin through 90° and visually dominated the fin's motion. Cupping had a significant effect on the shape of the fin, but the duration over which the leading edges of the fin were accelerated to put the fin into

the cupped configuration was short relative to the duration over which the fin was swept forward. Because of that, sweep is a more significant motion of the biorobotic fin and produces higher levels of drag than in the sunfish; so to be effective in the biorobotic fin, the cupping motion may have to be improved so that it accounts for a larger portion of the force, or it may only be effective when the other component motions produce lower forces such as when the fin is being moved slowly, or through small sweep angles.

Based solely on observation, we believe that the flexibility of the fin's distal end is an important element in the creation of thrust by cupping. The cupping motion is more pronounced at the base of the fin than it is at the fin's distal end. As the fin is cupped or opened, the distal end does not fold immediately about the spanwise axis, but seems to bend about the chord and create a small flapping motion. This motion could impart a thrust force onto the water. The flapping of the fin's distal end is, in fact, much more prominent in the movement of the sunfish pectoral fin than in the robotic fins, which lends support for it being an important factor in the production of thrust during the outstroke. This phenomenon is being investigated using a robotic fin that recreates the fish's cupping motion and its flexibility more exactly and that tunes the flexibility of the fin to create a resonant flapping as the fin is cupped and swept forward.

VII. Conclusion

This research used results from studies of the anatomy, kinematics, and hydrodynamics analyses of the bluegill sunfish pectoral fin to guide the design and build a biorobotic pectoral fin propulsor. The biological studies identified that the sunfish uses a complex pectoral fin motion during maneuvering and low-speed propulsion that is very different from the rowing and flapping models that have typically been used to describe pectoral fin swimming. The fin's movements are characterized by two leading edges that create leading edge vortices, a cupping of the fin about its spanwise axis, a dimpling along the upper surface that moves spanwise along the fin, a reorientation of the fin at its base, and significant area changes as the fin sweeps forward and back. These motions are due to the fish actively controlling the fin's shape and stiffness, and to a dynamic interaction between the fluid and the flexible fin. A result of this complex motion is that the fin produces relatively large positive thrust and small levels of lift and lateral forces during both the outstroke and instroke portions of the fin beat. Little energy is, therefore, wasted accelerating the fish up and down, laterally or backwards. Despite the complexity of the movements exhibited by the sunfish pectoral fin, the POD analysis indicated that it would be unnecessary to replicate the entire fin motion. CFD simulations indicated that cupping of the leading edges as the fin moved away from the fish body was instrumental in producing thrust during the outstroke, and that a majority of the thrust produced by the pectoral fin can be recovered using the gaits synthesized from the first few modes of POD analysis. These findings made it much simpler to define functional requirements for the robotic fin.

Although simple in structure relative to their biological counterparts, the components in the robotic fin served similar functions to those in the sunfish. The compliant mechanisms used in the biorobotic fin allowed the fin to move with many degrees of freedom, and the tendon and fin ray arrangement allowed there to be a high level of active control over the fin and its motion. The design successfully produced the four desired component motions—sweep, curl, expansion, and cupping—and enabled these component motions to be combined to produce more complicated movements that resembled those used by the sunfish. The fin was also able to create motions not typically used for propulsion by the sunfish, such as feathering and paddling, which demonstrated that a design such as this would allow a UUV to draw from a wide range of motions and use whichever was best suited for the particular task.

The sweep, curl, and expansion components affected the production of force in a manner that was expected. The force produced by the fin could be modulated by curl, which affected the fin's stiffness, and by expansion, which affected the fin's area. When added to other motions, cupping reduced the magnitude of the drag force, but did not cause the biorobotic fin to produce thrust during the outstroke as is done by the sunfish. This was possibly due to the drag from the other components being significantly greater than the thrust produced by the cupping motion. The results did show that when cupping was used alone, two positive thrust peaks were produced: one as the fin was cupped and another as the fin was opened. These results are very promising and require further study.

The study and analysis of the pectoral fin of the sunfish and the subsequent design and construction of a first generation biorobotic fin that can closely replicate the motions of the biological fin is an important first step towards developing propulsive devices that will give UUVs the ability to produce and control thrust like highly maneuverable fish.

Acknowledgment

The authors would like to thank Dr. T. McKenna of the U.S. Office of Naval Research and Dr. P. Bandyopadhyay of the U.S. Naval Undersea Warfare Center for their support and very helpful discussions.

References

[1] G. V. Lauder, "Locomotion," in *The Physiology of Fishes*, D. H. Evans and J. B. Claiborne, Eds., 3rd ed. Boca Raton, FL: CRC Press, 2005, pp. 3–46.

[2] G. V. Lauder and E. D. Tytell, "Hydrodynamics of undulatory propulsion," in *Fish Biomechanics*, R. E. Shadwick and G. V. Lauder, Eds. San Diego, CA: Academic Press, 2006, vol. 23, Fish Physiology, pp. 425–468.

[3] J. M. Anderson and N. K. Chhabra, "Maneuvering and performance of a robotic tuna," *Integr. Comp. Biol.*, vol. 42, pp. 118–127, 2002.

[4] S. Licht, V. Polidoro, M. Flores, and F. Hover, "Design and projected performance of a flapping foil AUV," *IEEE J. Ocean. Eng.*, vol. 29, no. 3, pp. 786–794, Jul. 2004.

[5] D. Beale and P. Bandyopadhyay, "Comparison of steady and unsteady hydrodynamics," in *Proc. 14th Int. Symp. Unmanned Untethered Submersible Technol.*, Durham, NH, 2005.

[6] B. C. Jayne, A. Lozada, and G. V. Lauder, "Function of the dorsal fin in bluegill sunfish: Motor patterns during four distinct locomotor behaviors," *J. Morphol.*, vol. 228, pp. 307–326, 1996.

[7] E. G. Drucker and G. V. Lauder, "A hydrodynamic analysis of fish swimming speed: Wake structures and locomotor force in slow and fast labriform swimmers," *J. Exp. Biol.*, vol. 203, pp. 2379–2393, 2000.

[8] E. G. Drucker and G. V. Lauder, "Wake dynamics and fluid forces of turning maneuvers in sunfish," *J. Exp. Biol.*, vol. 204, pp. 431–442, 2001.

[9] E. G. Drucker and G. V. Lauder, "Locomotor function of the dorsal fin in teleost fishes; experimental analysis of wake forces in sunfish," *J. Exp. Biol.*, vol. 204, pp. 2943–2958, 2001.
[10] G. V. Lauder and B. C. Jayne, "Pectoral fin locomotion in fish: Testing drag based model using three dimensional kinematics," *Amer. Zoologist*, vol. 36, pp. 567–581, 1996.
[11] G. V. Lauder and E. G. Drucker, "Morphology and experimental hydrodynamics of fish fin control surfaces," *IEEE J. Ocean. Eng.*, vol. 29, no. 3, pp. 556–571, Jul. 2004.
[12] J. D. Madden, N. A. Vandesteeg, P. A. Anquetil, P. G. Madden, A. Takashi, R. Z. Pytel, S. R. Lafontaine, P. A. Woeringa, and I. W. Hunter, "Artificial muscle technology: Physical principles and naval prospects," *IEEE J. Ocean. Eng.*, vol. 29, no. 3, pp. 706–728, 2004.
[13] J. A. Walker and M. W. Westneat, "Performance limits of labriform propulsion and correlates with fin shape and motion," *J. Exp. Biol.*, vol. 205, pp. 177–187, 2002.
[14] F. E. Fish and C. A. Hui, "Dolphin swimming—A review," *Mammal Rev.*, vol. 21, pp. 181–195, 1991.
[15] J. M. Anderson, K. Streitlien, D. S. Barrett, and M. S. Triantafyllou, "Oscillating foil of high efficiency," *J. Fluid Mech.*, vol. 360, pp. 41–72, 1998.
[16] J. A. Walker and M. W. Westneat, "Mechanical performance of aquatic rowing and flying," *Proc. R. Soc. Lond. B*, vol. 267, pp. 1875–1881, 2000.
[17] M. S. Triantafyllou, G. S. Triantafyllou, and D. K. P. Yue, "Hydrodynamics of fishlike swimming," *Annu. Rev. Fluid Mech.*, vol. 32, pp. 33–53, 2000.
[18] M. S. Triantafyllou, A. H. Techet, and F. S. Hover, "Review of experimental work in biomimetic foils," *IEEE J. Ocean. Eng.*, vol. 29, no. 3, pp. 585–594, Jul. 2004.
[19] I. Akhtar and R. Mittal, "A biologically inspired computational study of flow past tandem flapping foils," in *Proc. 35th AIAA Fluid Dyn. Conf. Exhibit 2005-4760*, Toronto, ON, Canada, 2005.
[20] E. M. Standen and G. V. Lauder, "Dorsal and anal fin function in bluegill sunfish Lepomis macrochirus," *J. Exp. Biol.*, vol. 208, pp. 2753–2763, 2005.
[21] P. J. Geerlink and J. J. Videler, "The relation between structure and bending properties of teleost fin rays," *Netherlands J. Zoology*, vol. 37, pp. 59–80, 1987.
[22] C. E. Willert and M. Gharib, "Digital particle image velocimetry," *Exp. Fluids*, vol. 10, pp. 181–193, 1991.
[23] R. Mittal and G. Iaccarino, "Immersed boundary methods," *Annu. Rev. Fluid Mech.*, vol. 37, pp. 239–261, 2005.
[24] M. Bozkurttas, H. Dong, V. Seshadri, R. Mittal, and F. Najjar, "Towards numerical simulation of flapping foils on fixed Cartesian grids," in *Proc. 43rd AIAA Aerosp. Sci. Meeting Exhibit 2005-0079*, Reno, NV, 2005.
[25] H. Dong, R. Mittal, M. Bozkurttas, and F. Najjar, "Wake structure and performance of finite aspect-ratio flapping foils," in *Proc. 43rd AIAA Aerosp. Sci. Meeting Exhibit 2005-0079*, Reno, NV, 2005.
[26] M. Narasimhan, H. Dong, R. Mittal, and S. Singh, "Optimal yaw regulation and trajectory control of bio-robotic AUV using pectoral fins based on CFD parameterization," *J. Fluid Eng.*, vol. 128, pp. 687–698, 2006.
[27] M. Bozkurttas, H. Dong, V. Seshadri, R. Mittal, and F. Najjar, "Towards numerical simulation of flapping foils on fixed Cartesian grids," in *Proc. 43rd AIAA Aerosp. Sci. Meeting Exhibit 2005-0079*, Reno, NV, 2005.
[28] M. Bozkurttas, H. Dong, R. Mittal, P. Madden, and G. Lauder, "Hydrodynamic performance of deformable fish fins and flapping foils," in *Proc. 44th AIAA Aerosp. Sci. Meeting Exhibit 2006-1392*, Reno, NV, 2006.
[29] R. Mittal, "Computational modeling in biohydrodynamics: Trends, challenges, and recent advances," *IEEE J. Ocean. Eng.*, vol. 29, no. 3, pp. 595–604, Jul. 2004.
[30] H. Dong, R. Mittal, and F. Najjar, "Wake topology and hydrodynamic performance of low aspect-ratio flapping foils," *J. Fluid Mech.*, vol. 566, pp. 309–343, 2006.
[31] K. Isogai, Y. Shinmoto, and Y. Watanabe, "Effects of dynamic stall on propulsive efficiency and thrust of flapping airfoil," *AIAA J.*, vol. 37, pp. 1145–1151, 1999.
[32] G. C. Lewin and H. Haj-Hariri, "Modeling thrust generation of a two-dimensional heaving airfoil in a viscous flow," *J. Fluid Mech.*, vol. 492, pp. 339–362, 2003.
[33] Y. C. Liang, H. P. Lee, K. H. Lee, and C. G. Wu, "Proper orthogonal decomposition and its applications—Part I: Theory," *J. Sound Vib.*, vol. 252, no. 3, pp. 527–544, 2002.
[34] A. V. Oppenheim, R. W. Schafer, and J. R. Buck, *Discrete-Time Signal Processing*, 2nd ed. Upper Saddle River, NJ: Prentice-Hall, 1999, pp. 474–478.
[35] M. Milano and M. Gharib, "Uncovering the physics of flapping plates with artificial evolution," *J. Fluid Mech.*, vol. 534, pp. 403–409, 2005.
[36] R. Ramamurti, W. Sandberg, B. Ratna, J. Naciri, and C. Spillman, "3-D unsteady computational investigations of the effect of fin deformation on force production in fishes," in *Proc. 14th Unmanned Untethered Submersible Technol. Symp.*, Durham, NH, Aug. 2004.
[37] A. B. Kessel, "Aerodynamics characteristics of dragonfly wing sections compared with technical airfoils," *J. Exp. Biol.*, vol. 203, pp. 3125–3135, 2000.
[38] N. Kato, "Control performance in the horizontal plane of a fish robot with mechanical pectoral fins," *IEEE J. Ocean. Eng.*, vol. 25, no. 1, pp. 121–129, Jan. 2000.
[39] A. Techet, K. Lim, F. Hover, and M. Triantafyllou, "Hydrodynamic performance of a biologically inspired three-dimensional flapping foil," in *Proc. 14th Int. Symp. Unmanned Untethered Submersible Technol.*, Durham, NH, 2005.

James Louis Tangorra (M'03) received the B.S. and M.Eng. degrees in mechanical and aerospace engineering from Cornell University, Ithaca, NY, in 1989 and 1990, respectively, and the Ph.D. degree in mechanical engineering from the Massachusetts Institute of Technology (MIT), Cambridge, in 2003.

He was an Engineering Officer in the U.S. Navy from 1990 to 1996, and in the U.S. Navy reserves from 1997 to 2007. He was a Postdoctoral Researcher at the Bioinstrumentation Laboratory, MIT, from 2004 to 2007. Currently, he is an Assistant Professor of Mechanical Engineering at Drexel University, Philadelphia, PA. His research focuses on the use of system level engineering analysis techniques to understand the functional performance of biological systems.

S. Naomi Davidson received the B.S. degree in mechanical engineering from the University of California at Berkeley in 2002 and the M.S. degree in mechanical engineering from the Massachusetts Institute of Technology (MIT), Cambridge, in 2005.

Currently, she is a Management Consultant for McKinsey and Company.

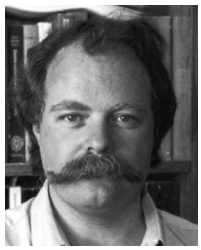

Ian W. Hunter was born in New Zealand in 1953. He received the B.Sc., M.Sc., D.C.P., and Ph.D. degrees in science from the University of Auckland, Auckland, New Zealand, in 1974, 1975, 1976, and 1980, respectively.

He was with McGill University, Montreal, QC, Canada, from 1980 to 1994, when he joined the faculty of Massachusetts Institute of Technology (MIT), Cambridge, where he is currently the Hatsopoulos Professor of Mechanical Engineering. His current research interests are microinstrumentation, microfabrication, microrobotics, microsurgical robotics, artificial muscle fibers, laser imaging systems, and instrumentation physics.

Peter G. A. Madden was born in Ottawa, ON, Canada, in 1971. He received the B.A.Sc. degree in engineering physics from the University of British Columbia, Vancouver, BC, Canada, in 1993, the M.Eng. degree in biomedical engineering from McGill University, Montreal, QC, Canada, in 1996, and the Ph.D. degree in mechanical engineering from the Massachusetts Institute of Technology (MIT), Cambridge, in 2003.

Currently, he is process engineering for Evergreen Solar, Inc., Marlboro, MA.

George V. Lauder received the A.B. and Ph.D. degrees in biology from Harvard University, Cambridge, MA, in 1976 and 1979, respectively.

From 1979 to 1981, he was a Junior Fellow in the Society of Fellows, Harvard University. He then joined the faculty at the University of Chicago, Chicago, IL, and in 1986, the Department of Ecology and Evolution at the University of California, Irvine. Since 1999, he has been the Alexander Agassiz Professor of Zoology and Professor of Organismic and Evolutionary Biology at Harvard University. His research interests focus on the biomechanics and evolution of fishes, with a special focus on laboratory analyses of kinematics, muscle function, and hydrodynamics of freely swimming fishes. His current work involves application of analyses of fish locomotor function to the design of biorobotic underwater vehicles.

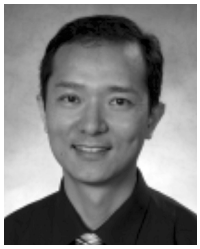

Haibo Dong received the Ph.D. degree in aerospace engineering from The University of California, Los Angeles, in 2002.

Then, he joined the George Washington University, Washington, DC, as a Research Scientist and conducted research in the area of computational biological flow. Currently, he is an Assistant Professor at the Department of Mechanical and Materials Engineering, Wright State University, Dayton, OH. His research interests include computational fluid dynamics, biofluid dynamics, aerodynamics, fluid–structure interaction, and microaerial vehicles.

Meliha Bozkurttas received the B.S. and M.S. degrees in aeronautical engineering from Middle East Technical University (METU), Ankara, Turkey, in 1998 and 2001, respectively, and the Ph.D. degree in mechanical and aerospace engineering from the George Washington University, Washington, DC, in 2007.

She was a Graduate Research Assistant in Flow Simulation and Analysis Group at the George Washington University from 2002 to 2007. Currently, she is an Application Engineer at Exa Corporation. Her research interests are in unsteady fluid dynamics, fluid–structure interaction, and biological flows.

Rajat Mittal received the B.Tech. degree in aeronautical engineering from Indian Institute of Technology, in 1989, the M.S. degree in aerospace engineering from University of Florida, Gainesville, in 1991, and the Ph.D. degree in applied mechanics from University of Illinois at Urbana-Champaign, Urbana, in 1995.

Since 2001, he has been a Professor at the Department of Mechanical and Aerospace Engineering, The George Washington University, Washington, DC. He was an Assistant Professor at the Department of Mechanical Engineering, University of Florida, for five years. In 1995, he joined the Center for Turbulence Research at Stanford University, Stanford, CA, as a Postdoctoral Fellow. For the past fifteen years, his research work has focused on DNS/LES of complex flows, fluid–structure interaction, biological flows, and active flow control.